Seasonal effects of the Tibetan plateau on the cyclonic transient eddies: a system-centered view

Article

Accepted Version

Seasonal Effects of the Tibetan Plateau on Cyclonic Transient Eddies: A System- centered View

QIAOLING REN[a], KEVIN I. HODGES[b], REINHARD SCHIEMANN[b], YONGJIU DAI[a,c], XINGWEN JIANG[d], AND SONG YANG[a,c*]

[a] *School of Atmospheric Sciences, Sun Yat-sen University; Southern Marine Science and Engineering Guangdong Laboratory (Zhuhai), Guangdong, China*

[b] *National Centre for Atmospheric Science, University of Reading, Reading, United Kingdom*

[c] *Guangdong Province Key Laboratory for Climate Change and Natural Disaster Studies, Sun Yat-sen University, Zhuhai, Guangdong 519082, China*

[dc] *Institute of Plateau Meteorology, China Meteorological Administration, Chengdu, Sichuan, China*

Revised for *Journal of Climate*

June 2023

**Corresponding author & address:* Prof. Song Yang, School of Atmospheric Sciences, Sun Yat-sen University, 2 Daxue Road, Zhuhai, Guangdong 519082, China. E-mail: yangsong3@mail.sysu.edu.cn

ABSTRACT

Using an objective feature tracking algorithm and ECMWF fifth-generation hourly reanalysis data (ERA5), the seasonal behaviors of cyclonic transient eddies (cyclones) at different levels around the Tibetan Plateau (TP) were examined to understand the effects of the TP on cyclones. Results show that the TP tends to change the moving directions of the remote cyclones when they are close to the TP, with only 2 percent of the 250-hPa eastward-moving cyclones directly passing over the TP. The sudden reductions of their moving speeds and relative vorticity intensities around the TP suggest a suppression effect of the plateau. Over 70 percent of these cyclones perish over the TP regardless of the altitude. This percentage decreases to around 65 percent during summertime, exhibiting a weaker summer suppression effect. On the other hand, the TP has a stimulation effect on local cyclones through its dynamic forcing in winter, thermodynamic forcing in summer, and both forcings in the transitional seasons. The numbers of locally-generated cyclones, especially at 500 hPa, just above the TP, are significantly larger than those of the remote cyclones during all seasons. Although about half of the local cyclones dissipate over the TP, the cyclones moving off the plateau significantly outnumber the moving-in cyclones, with the differences ranging from 0 to 6 cyclones per month. Only the 250-hPa wintertime moving-off cyclones are fewer than the cyclones entering the TP, which may be caused by the weaker stimulation effect and stronger suppression effect of the TP on the wintertime upper-level cyclones.

SIGNIFICANCE STATEMENT

Cyclonic transient eddies (cyclones), steered by westerly jet streams, can influence climate and induce extreme weather processes under certain conditions. Tibetan Plateau (TP), the highest and largest obstacle embedded in the westerly jet streams, suppresses the remote cyclones entering the TP region, destroying over 70 percent of these cyclones. However, due to the excitation effect of the TP on local cyclones, the numbers of cyclones moving off the TP are still larger than or equal to

those of the moving-in cyclones, except at the upper levels in winter. This feature suggests that the TP cannot significantly decrease the total cyclone numbers in most cases, but it indeed weakens the mean intensity and moving speed of the cyclones.

1. Introduction

Transient eddies (TEs), an important part of the atmospheric circulation, are cyclonic or anti-cyclonic disturbances that move with the background flow, including extratropical cyclones, westerly troughs, shear lines, and other types of weather systems. They can influence the global climate through the transport of energy and matter (Peixoto and Oort 1992; Lorenz and Hartmann 2003; Ren et al. 2022) and are also an important factor affecting local weather processes (Liu et al. 2018; Zhao et al. 2020). The occurrence and development of TEs are affected by various factors such as the westerly jet streams, diabatic heating, and topography (Chang et al. 2002; Kang and Son 2021). In particular, topography as a long-standing fixed external forcing can significantly affect TEs in a variety of ways, including topographic drag (Ólafsson and Bougeault 1997), mechanical obstruction (Son et al. 2009), altered temperature field (Davis 1997), and orographically forced stationary waves (Yu and Hartmann 1995; Park et al. 2013). Topographic effects substantially depend on the mountain size, shape, and height as well as the background flow (Qian and Jiao 1995; Yu and Hartmann 1995; Son et al. 2009). Thus, the interaction between topography and TEs has always been a key issue in global meteorological research.

As a zonally-extending terrain with the highest average elevation and largest area in the world, the Tibetan Plateau (TP) is linked to the Hengduan Cordillera to the east, the Iranian Plateau to the west, the Mongolian Plateau to the north, and the Indian Ocean with abundant water vapor to the south. Thus, the topography around the plateau is remarkably complex. Numerous studies have shown the vital roles played by the TP in global climate through thermal forcing in summer and mechanical forcing in winter (Molnar et al. 2010; Wu et al. 2007, 2012, 2015). In addition, the meridional location of the TP is the key latitude for the seasonal evolution of the westerly jet stream. From winter to summer, the jet stream moves from the south to the north of the TP, and it moves oppositely from summer to winter (Schiemann et al. 2009), indicating the varying background flow around the plateau. As the westerly jet stream is an important waveguide and a region that tends to generate TEs, it is necessary to investigate the

seasonal effects of the TP on TEs.

Based on numerical experiments with and without the TP in a dry global general circulation model (GCM), Chang (2009) noted that the existence of this large terrain could significantly suppress the activity of TEs in winter. Park et al. (2010) and Lee et al. (2013) obtained a similar result through changing the height of the TP respectively in an atmospheric GCM and in a coupled atmosphere-ocean GCM, and further found that the suppression effect became weaker in other seasons. They argued that the weakened eddy seeding-feeding process (Zurita-Gotor and Chang 2005; Penny et al. 2010) induced by the suppression effect of the TP played a role in the midwinter suppression of the North Pacific storm track, which is a striking phenomenon that TE activities over the North Pacific are weaker in winter than in fall and spring even though the low-level baroclinicity peaks in winter (Park et al. 2010; Lee et al. 2013). Ren et al. (2021) used a nudging method to modify the suppression effect of the TP on TEs in the NCAR Community Earth System Model and discovered that the suppression effect could significantly influence East Asian rainfall in early summer through weakening the westerly jet stream.

Nevertheless, several issues in these insightful studies need further explanations. First, most of their conclusions were obtained based on numerical simulations, which are sensitive to the models applied (Chang and Lin 2011). Secondly, their results were mainly based on the Eulerian method of TE diagnosis, using the bandpass-filtered variance field. This method can easily provide a general measure of TEs, and can be used in atmospheric heat and momentum budget analyses. However, it cannot show the features of the frequency, intensity, moving speed, generation, and dissipation situations of each individual eddy, which can be obtained from system-centered methods (Hoskins and Hodges 2002; Penny et al. 2010). Thirdly, these studies have mainly focused on the TEs in the upper troposphere, neglecting the effects of the TP on the mid- and lower-level TEs while the TP is a large topography soaring into the middle troposphere. Thus, a study using observed data and system-centered methods to explore the effects of the TP on the TEs at different altitudes is still needed, which is the motivation of this study.

Existing studies from a system-centered perspective often have been focused on

the particular types of observed TEs around the TP. For example, based on one-year 500-hPa geopotential height data over 50-60°N, Yeh (1952) noted that most wintertime low-pressure troughs cannot move across the plateau from the west to the east, which may be related to the semi-permanent high-pressure ridge induced by the deflection of the westerly jet stream impinging upon the TP. In summer, the high-pressure ridge to the north of the TP disappears with the northward movement of the jet stream, and more low-pressure troughs can move across the plateau. Jiao and Qian (1994) utilized the 500-hPa daily historical synoptic maps around the TP for 5 winters to count the activities of eastward-moving troughs, whose meridional length is larger than 10 degrees. They found that these troughs often slow down, weaken, and even disappear, when they approach the western side of the TP, also suggesting the suppression effect of the TP. Some studies have been focused on the behaviors of westerly disturbances that account for over 50% of the total annual precipitation in western Himalaya and Karakoram (Cannon et al. 2016; Hunt et al. 2018; Javed et al. 2022), and the Central Asian vortexes that can have severe impacts such as rainstorms, snowstorms, and low temperatures to the northwest of the TP (Zhang et al. 2012; Zhuang et al. 2017). Since these studies employ a range of different methods and terminologies, a coherent analysis for all kinds of TEs around the TP region is called for.

Moreover, the above studies have mainly concentrated on the eastward moving eddies influenced by the TP; however, there are many TEs generated around the TP due to the widely accepted lee cyclogenesis theory and the cyclonic shear induced by the topographic drag, such as the TP shear lines and the southwest vortexes (Wang 1954; Guan et al. 2018; Li and Zhang 2019). Other studies also argued that the diabatic heating forced by high topography in summer was necessary for the generation of TP vortices (Zhang et al. 2021; Ma et al. 2022), which can induce heavy rainfall locally and downstream (Wang 1987; Li et al. 2014; Curio et al. 2019). Previous studies also prove that the north-south dipole precipitation trend over the TP is closely linked to the activities of TP vortices (Li et al. 2021; Li and Zhang 2023). These studies hint the stimulation effect of the TP on local generation of TEs, which may be different from the effects of the TP on the remote eddies propagating from outside. Thus, several

146 questions arise naturally. 1) How do the effects of the TP on the remote and local TEs
147 change with altitudes and seasons? 2) What are the differences between these effects?
148 To answer the above questions, an objective feature tracking algorithm is applied
149 to a high-resolution reanalysis dataset to analyze and quantify the seasonal behaviors
150 of the remote and locally-generated TEs around the TP at three commonly used pressure
151 levels (850, 500, and 250 hPa) focusing on their generation, dissipation, moving path,
152 and intensity variation. This analysis can reveal the detailed manifestations of the
153 effects of the TP on TEs. Examining the seasonal cycle is also helpful for understanding
154 how the effects of the TP on TEs are related to the winter-dominated dynamic and
155 summer-dominated thermal effects of the TP and the north-south movement of the jet
156 stream over the TP. According to Hoskins and Hodges (2002), cyclonic eddies are
157 stronger than anti-cyclonic eddies, and can almost reflect the characteristics of TEs
158 highlighted by the Eulerian method. Combined with the fact that many impactful TEs
159 around the TP are cyclonic eddies, this paper is focused on the cyclonic eddies, which
160 are referred to as cyclones below for the sake of convenience. The used data and feature
161 tracking method are introduced in section 2. Seasonal effects of the TP on the remote
162 and locally-generated cyclones are described and compared in section 3. Results are
163 summarized and discussed in section 4.
164

165 ## 2. Data and methodology

166 The data used in this study comes from the fifth-generation European Centre for
167 Medium-range Weather Forecast (ECMWF) atmospheric reanalysis (ERA5), which
168 provides a much higher temporal and spatial resolution than the previous reanalysis
169 datasets. It is the latest global climate and weather reanalysis based on the Integrated
170 Forecasting System Cy41r2 that exhibits large improvements in model physics, core
171 dynamics, and data assimilation over earlier versions. Vast amounts of historical
172 observations have been combined into the ERA5 via 4D-Var data assimilation with a
173 12-h window and variational bias correction. Hourly atmospheric products with a
174 horizontal resolution of 31 km and 137 levels spanning from land surface to 0.01 hPa

are available from the ERA5, which can capture much finer details of atmospheric phenomena (Hersbach et al. 2020).

To identify and track cyclones, the objective feature tracking algorithm developed by Hodges (1994, 1995, 1999) is used, which can be flexibly adapted to track different systems based on different fields and constraints, and has been used in previous studies of midlatitude cyclones (Hoskins and Hodges 2002, 2005), tropical cyclones (Hodges et al. 2017; Studholme et al. 2022), TP vortices (Curio et al. 2018, 2019). Any suitable field can be used with the algorithm but usually the sea level pressure, 500-hPa geopotential height, or relative vorticity is used. The relative vorticity is usually used as it is less influenced by the large-scale background flow. Moreover, it can focus on more smaller scales to allow systems to be identified much earlier in their life cycles (Hoskins and Hodges 2002). As there may be many small-scale cyclones induced by the TP, hourly ERA5 relative vorticity fields from 1979 to 2021 at 850, 500 and 250 hPa have been chosen to identify the cyclones around the TP. The 500 hPa level is just above the surface of the TP, while the 850 and 250 hPa levels are typical representatives of the lower and upper atmosphere.

Since the relative vorticity at high resolution is a very noisy field, it is first spectrally filtered to T63 to remove small-scale noise. The large-scale background with total wavenumbers n<=5 is also removed to focus on synoptic-scale cyclones. Then, the objective feature tracking algorithm identifies cyclone centers as the off-grid maxima above a threshold of 1.0×10^{-5} s^{-1} for all three levels using the B-spline interpolation and a steepest ascent/descent optimization (Hodges 1995). Next, the tracking is performed by first initializing as set of tracks by linking the identified cyclone centers together in a time order using a nearest-neighbor approach. These tracks are then refined through the minimization of a cost function for track smoothness based on direction and speed, using adaptive constraints for displacement distance and track smoothness (Hodges 1994, 1999). In general, the higher the temporal resolution, at a fixed spatial resolution, the more reliable the cyclone tracking might be expected to be (Curio et al. 2018). Although this paper is focused on the cyclones around the TP, the cyclones throughout the whole northern hemisphere have been tracked to ensure the

integrity of the cyclones through their life history, especially those with long lifetimes and long travel distances. Besides, the cyclones that persist for at least one day and travel more than 500 km have been chosen to focus on the mobile cyclones.

Then, cyclones interacting with the TP have been selected by choosing those whose shortest distance from the TP is less than the cyclone size. Among these selected cyclones, if the shortest distances between the cyclone genesis points and the TP are less than their cyclone sizes, these cyclones are further defined as local cyclones generated over the TP, while the others are the remote cyclones that are created at other places but can pass over the TP. Similarly, a cyclone with the shortest distance between its cyclolysis point and the TP less than the cyclone size is regarded as a cyclone dying over the TP, while the others are the cyclones that can move out of the TP. Here the TP is defined as the region bounded by 23~45°N/60~110°E, and where the altitude is higher than 1500 m, excluding the Mongolian Plateau. The cyclone size varies with the type, development stage, and geographic location of the cyclone (Hawcroft et al. 2012; Zappa et al. 2015; Curio et al. 2019). There are various methods to define the cyclone size, but none can accurately measure it (Rudeva and Gulev 2007; Dai and Nie 2022). Considering that the cyclones analyzed in this study involve both the small-scale TP vortices and the mesoscale extratropical cyclones, the cyclone size is roughly set at 6° to define the remote cyclones that move into the TP, locally-generated cyclones over the TP, and the cyclones that dissipate over the TP, Besides, the cyclone size of 3° has also been used to select the above cyclones and similar results have been obtained (not shown).

Similar to previous studies, the climatological spatial statistics are calculated from the cyclone tracks to produce track, genesis, and lysis densities using the spherical kernel approach (Hodges 1996). The genesis (lysis) density is calculated from the starting (ending) point of a cyclone lifetime excluding any cyclones that start (end) at the first (last) time step, while the track density refers to the number of cyclones per unit area passing through a region. The units of these densities are the number per month per unit area that is equivalent to a 5° radius spherical cap, an area of about 10^6 km^2. Note, that regions of high density just mean the preferred regions for cyclones to occur,

and individual cyclones can also appear in other regions. Mean attributes of cyclones over particular regions have also been calculated, including intensity, moving speed, growth rates, and lifetime. Since attributes calculated from a small sample are less reliable, results where the track densities are lower than one cyclone per month per unit area are not shown in the following figures.

3. Results

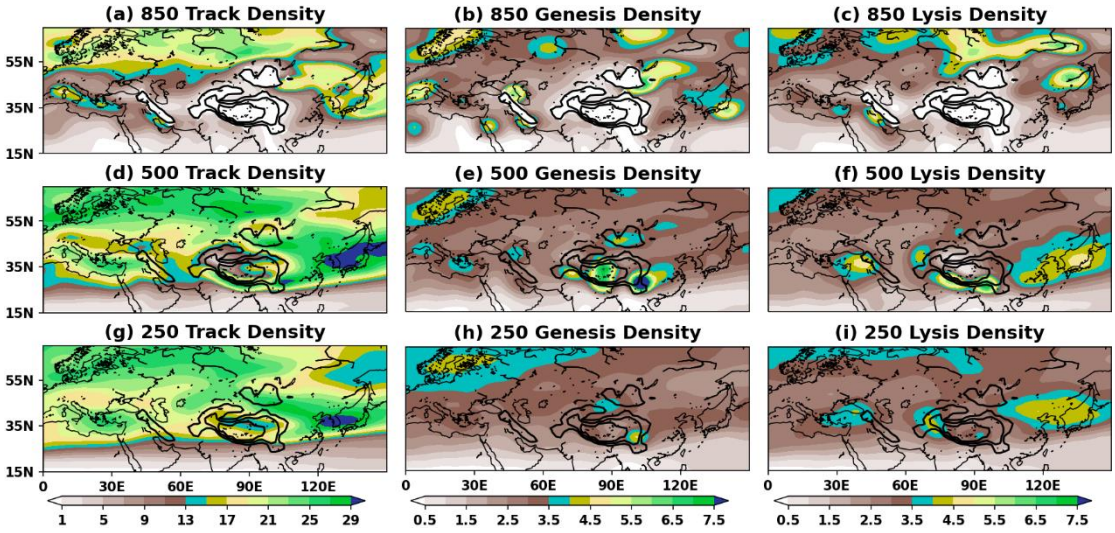

FIG. 1. Annual average (left) track, (center) genesis, and (right) lysis densities (shading; the number of cyclones per month per unit area) of all (upper) 850-hPa, (middle) 500-hPa, and (bottom) 250-hPa cyclones. Thick black contours indicate the elevation of 1500, 3000, and 4500 m.

Before focusing on the cyclones passing through the plateau, the annual average distribution of all cyclones in an extended region are shown in Fig. 1 to help us understand the roles played by the TP in the cyclones. It can be seen that the track densities at all altitudes are large over northern Europe, western Russia, East Asia, and the Mediterranean, consistent with previous studies (Hoskins and Hodges 2002). These track densities fall away rapidly to the south due to the weak baroclinicity at low latitudes. Close to the TP, the 850-hPa track densities suddenly decrease to a value less than 3 cyclones per month per unit area (Fig. 1a). Variations in the 500-hPa track densities are more dramatic when the tracks encounter the TP, decreasing from 15 to 3

over a small distance. However, the lowest 500-hPa track density is mainly confined to the western TP while it starts to increase over the eastern TP (Fig. 1d). The 250-hPa track densities over the TP have the lowest value around 11 over a small area of the northern TP, but are larger than those at 500 hPa (Fig. 1g), hinting that there may be more cyclones passing through the TP at the upper levels.

Due to the complex topography near the surface, several high 850-hPa genesis density regions can be seen around the Scandinavian Peninsula, the Alps, the Ural Mountains, the Caspian Sea, the southwestern Iranian Plateau, the central Sibirian Plateau, the Mongolian Plateau, and southern Japanese Island, all of which decrease with altitude (middle column in Fig. 1). However, there are two high 500-hPa genesis densities over the southeastern and central TP, much stronger than the others, signifying the stimulation effect of the TP on local cyclogenesis. High genesis density region over the southeastern TP can extend to the upper level while that over the central TP disappears at 250 hPa (Figs. 1e and h), implying that the local cyclones generated over the central TP may be mostly shallow systems. Besides, it is apparent that the western and southern borders of the TP are the main cyclolysis regions (except for East Asia and the Iranian Plateau), where 500- and 250-hPa cyclolysis occurs frequently (Figs. 1f and i), further suggesting the suppression effect of the TP on the remote cyclones entering the TP region. The fact that the 850-hPa lysis densities around the TP are lower than those over Russia may be related to the small track densities around the TP at this level (Fig. 1c).

In general, Fig. 1 shows that the TP exerts a suppression effect on remote cyclones and a stimulation effect on local cyclones. To evaluate and compare these two effects, Fig. 2 shows the numbers of the remote and local cyclones per season as well as the percentages of those cyclones dying over the TP. Clearly over 73% of the wintertime remote cyclones die out over the TP regardless of the altitude, and the percentage gradually drops to around 64% in summer, exhibiting a weak summertime suppression effect (Fig. 2a). The numbers of local cyclones are always larger than those of remote cyclones. While the numbers of remote cyclones increase with altitude for all seasons, consistent with the track densities shown in Fig. 1, the numbers of local cyclones are

always largest at 500 hPa, consistent with Fig. 1e, suggesting a strong stimulation effect just above the surface of the TP. The numbers of local cyclones at all three levels are maximized in spring and minimized in summer, while the numbers of remote cyclones peak in winter, highlighting a particular seasonal variation of the stimulation effect (Fig. 2). To further understand the detailed manifestations of these two effects and their seasonal variations, the seasonal behaviors of the remote and local cyclones are further examined below.

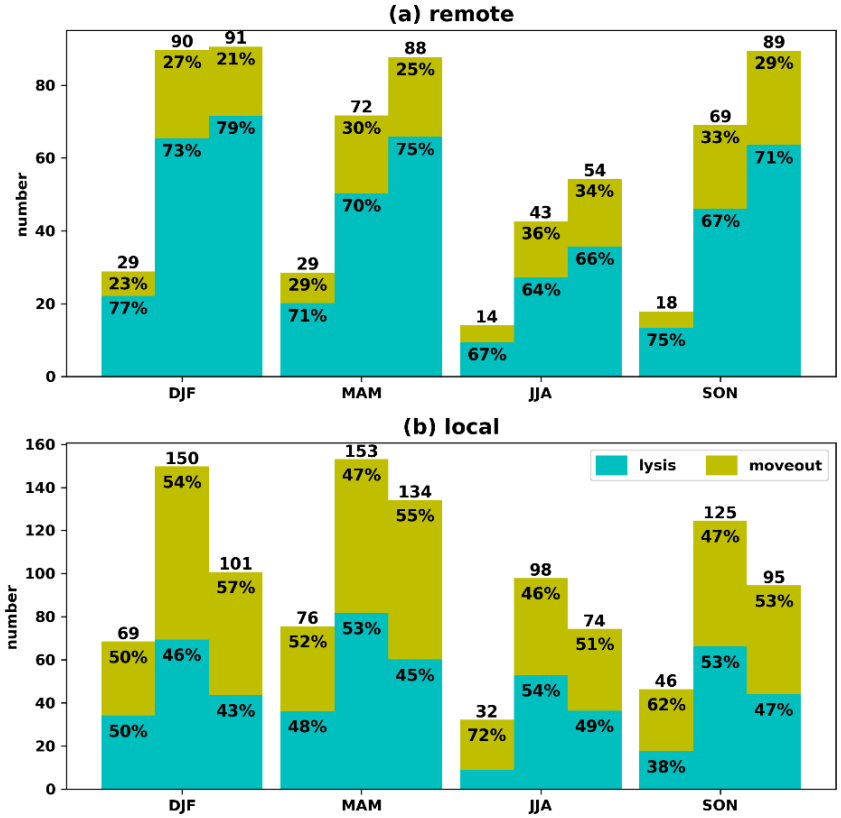

FIG. 2. Numbers of (a) remote cyclones moving eastward into the TP and (b) local cyclones generated around the TP per season, averaged over 41 years, with the three bars in each season representing the 850-, 500-, and 250-hPa cyclones, respectively. Cyan parts represent the cyclones that dissipate over the TP while yellow parts signify the cyclones that move out of the TP. Their percentages relative to the total numbers of cyclones at each level for each season, which are denoted on the top of each bar, are marked in each part if the percentages are large enough.

a. TP effects on remote cyclones

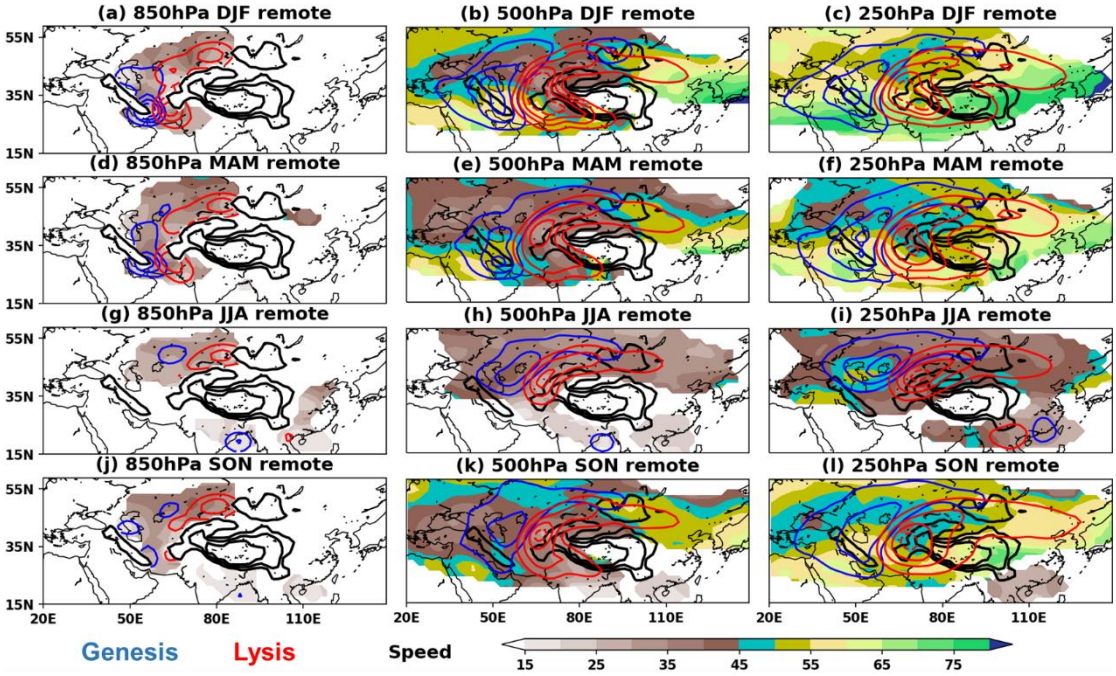

FIG. 3. Climatological genesis densities (blue contours), lysis densities (red contours) and mean phase speeds (shading; $m\ s^{-1}$) of (left) 850-hPa, (center) 500-hPa, and (right) 250-hPa remote cyclones for each season: (first row) winter, (second row) spring, (third row) summer, and (fourth row) autumn. Contour values are 1, 2, 3, 4 (dashed), 7, 10, and 13 cyclones per month per unit area for both blue and red contours. Mean phase speed is not shown for track densities below 1. Thick black contours indicate the elevation of 1500, 3000, and 4500 m.

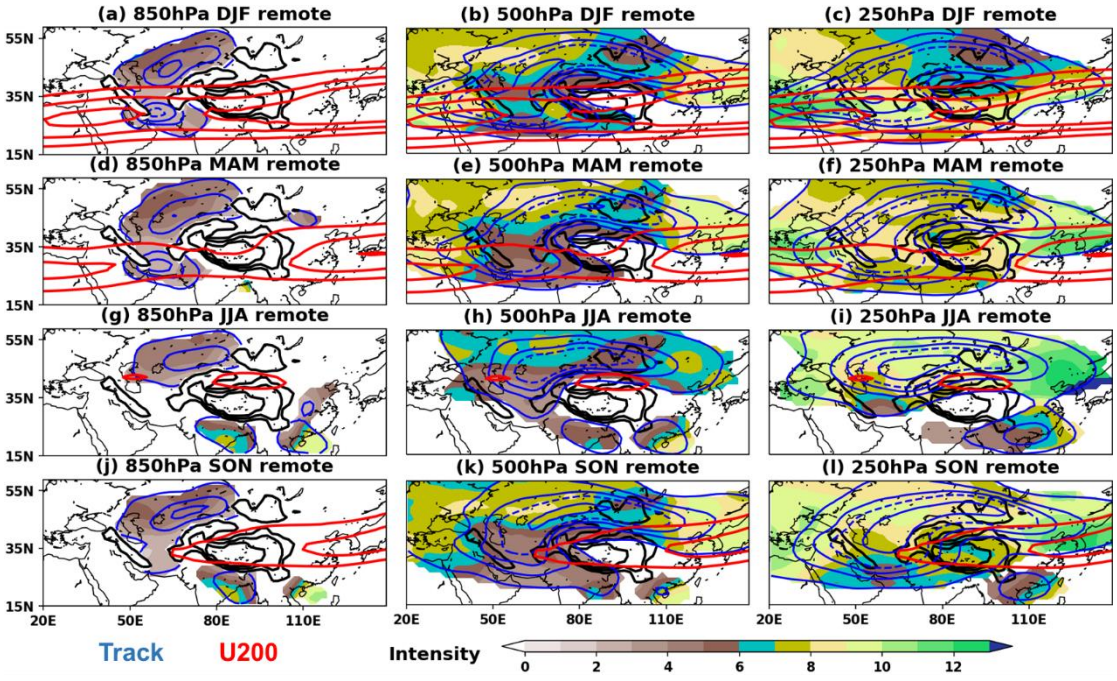

FIG. 4. Climatological track densities (blue contours) and mean intensities (shading; $10^{-5}\ s^{-1}$) of (left) 850-hPa, (center) 500-hPa, and (right) 250-hPa remote cyclones for each season: (first row) winter, (second row) spring, (third row) summer, and (fourth row) autumn. Track density contours are 1, 3.5, 6, 8.5 (dashed), 13.5, and 18.5 cyclones per month per unit area. Mean intensity is not shown for track densities below 1. The 200-hPa westerly jet stream is indicated using the 30, 40, and 50 m/s red contours of 200-hPa zonal wind. Thick black contours indicate the elevation of 1500, 3000, and 4500 m.

Previous studies have shown that the westerly jet stream, together with strong atmospheric baroclinicity, is closely related with cyclone intensities and can influence the trajectories and moving speeds of cyclones (Chang et al. 2002; Holton 2004). Thus, the seasonal characteristics of the remote cyclones and the 200-hPa westerly jet stream are displayed in Figs. 3 and 4. As shown in Fig. 3a, the preferred genesis region for wintertime 850-hPa remote cyclones is the leeside of the Iranian Plateau (see blue contours), with a maximum genesis density to the southeast of the Iranian Plateau, consistent with the lee cyclogenesis theory. These cyclones mainly die out to the west of the TP, along the 1500-m isohypse, with high lysis densities over the southwestern

and northwestern corners of the TP and the upstream region of the Mongolian Plateau (Fig. 3a). This configuration suggests that the low-level cyclones tend to turn north or south when they encounter the TP, exhibiting as two bands of high track densities relatively located to the north and south of the TP (blue contours in Fig. 4a). This feature reflects the diversion effect of the TP on remote cyclones. Due to the blockage of the TP, the activities of low-level cyclones are mainly confined to the west of 90°E.

At the middle and higher levels, the spatial distributions of remote cyclones are similar to those of the low-level cyclones, but covering a larger area. Specially, the preferred genesis regions extend further westward to the Mediterranean and northeastward to the Mongolian Plateau. The preferred lysis regions spread to 117°E for the northern branch and 92°E for the southern branch, with the highest lysis densities to the west of the TP. This feature of distribution appears like a letter "C", but with a longer upper branch (Figs. 3b and c). The northern and southern branches thus have higher track densities and longer moving distances than those of the low-level cyclones. Some northern cyclones can move into East Asia (Figs. 4b and c). It is worth noting that there are also no values over the central TP at the 500hPa, suggesting that no cyclone can move across the TP in this level while some 250-hPa cyclones can do this. However, more cyclones die over the TP at 250 hPa (79%) than at 500 hPa (73%), which is also observed in the other seasons (Fig. 2a). It suggests that the diversion effect of the TP decreases with altitude, leading to more 250-hPa cyclones directly moving into the TP and dying over the plateau. Only about 2 percent of the upper-level cyclones that can move eastward to East Asia across the TP.

Consistent with the seasonal variation of the background flow (Fleming et al. 1987), the distributions of remote cyclones in spring are similar to those in winter but with slightly weaker maximum densities (first two rows in Figs. 3 and 4). In summer, due to the northward shift of atmospheric baroclinicity, reflected in the westerly jet stream, the preferred activity regions for the remote cyclones entering the TP shrink to the north, and the southern branch disappears. Thus, the diversion effect of the TP becomes weak in summer. The weakened gradients of the track densities to the west of the TP in summer also suggest a weak suppression effect of the TP, which is also reflected in Fig.

2a. The decreased distances traveled by the remote cyclones may be related to their weak intensities and small moving speeds, which result from the weak baroclinicity and slow background flow in summer. Besides, some tropical cyclones are generated over the Bay of Bengal and the South China Sea, and they move eastward to interact with the TP under the control of the tropical easterly jet stream (third row in Figs. 3 and 4). The behaviors of the remote cyclones in autumn are comparable to the conditions in spring, but with fewer southern cyclones (fourth row in Figs. 3 and 4). Furthermore, it can be seen that the spatial and temporal distributions of remote cyclones are consistent in all three levels (Figs. 3 and 4), implying the high probability for deep cyclones to occur in the remote cyclones.

In addition to the decrease in cyclone densities over the TP, the effects of the TP on the remote cyclones are also reflected in their sudden decrease in moving speeds and relative vorticity intensities around the TP, shown as the shadings in Figs. 3 and 4. The decrease in moving speeds mainly occurs upstream of the TP and the Mongolian Plateau, overlapping the increase in their lysis densities at all three levels and during all seasons, further reflecting the blocking effect of the topography (Fig. 3). Since the moving speeds depend on the background flow, northern cyclones accelerate when they move into the westerly jet stream after bypassing the TP from the north (Figs. 3b, c, e, f, k, and l). This feature also explains that the summertime upper-level remote cyclones accelerate to the north of the TP (Fig. 3i) and that the southern branch, co-located with the westerly jet stream, has a larger moving speed than the northern branch in the middle and high levels during winter and spring (Figs. 3b, c, e, and f).

Decreases in the relative vorticity intensities appear to the west of the TP at the low and middle levels, co-located with the westerly jet stream where the atmospheric baroclinicity is strong (Fig. 4), signifying a strong suppression effect of the TP. This phenomenon is noticeable during all seasons except summer when the southern branch disappears and the traveled distances of remote cyclones are short due to the weak westerly jet stream (third row in Fig. 4). Besides, another weakening feature appears over the Mongolian Plateau at 500 hPa during all seasons (middle column in Fig. 4), possibly by the Mongolian Plateau or TP induced northern high-pressure ridge, as

393 suggested by Yeh (1952). This weakening is also marked at 250h Pa during winter and
394 spring (Figs. 4c and f), when the TP induced northern high-pressure ridge is strong due
395 to the powerful westerly jet stream. Consistent with the variation of the moving speeds,
396 there is an increase in the cyclone intensities over northern East Asia. In addition, the
397 intensities of winter and spring southern cyclones undergo a re-intensification to the
398 southwest of the TP in all levels especially at 500 hPa (Figs. 4b and e). This feature may
399 be induced by latent heat feedback, since the southern cyclones in winter and spring
400 can carry ample water vapor from the Mediterranean, the Red Sea, Persian, and the
401 Arabian Seas, which is blocked by the TP to produce heavy precipitation to the
402 southwest of the TP (Cannon et al. 2016).
403
404 *b. TP effects on local cyclones*
405 The seasonal average genesis densities of the local cyclones generated over the TP
406 are shown in Fig. 5. There are two areas of high genesis densities over the southeastern
407 corner and the southernmost border of the TP during winter, which exists in all three
408 levels but with a maximum at 500 hPa (first row in Fig. 5), consistent with Fig. 2b.
409 According to previous studies, the former preferred genesis region may be related to
410 the enhancement of potential vorticity caused by the stretched air column downstream
411 of the plateau (Holton 2004; Wang and Tan 2014), while the latter may be produced by
412 the friction and topographic drag induced cyclonic shear under the background of
413 strong westerly winds (Wang 1954; Luo and Wei 1985). One may argue about the role
414 of atmospheric baroclinicity in the cyclogenesis, but the spatial distribution of genesis
415 densities around TP is inconsistent with the meridional gradient of potential
416 temperature (not shown), hinting that the above two high genesis densities are both
417 dynamically induced. These two mechanisms can also be applied to explain the above-
418 mentioned re-intensification of the southern remote cyclones in the small open area
419 behind the southwestern corner of the TP (Figs. 4b and e). Besides, another 850-hPa
420 cyclogenesis preferred area is located downstream of the Mongolian Plateau (Fig. 5a),
421 which can be viewed as the lee cyclogenesis of the Mongolian plateau.
422

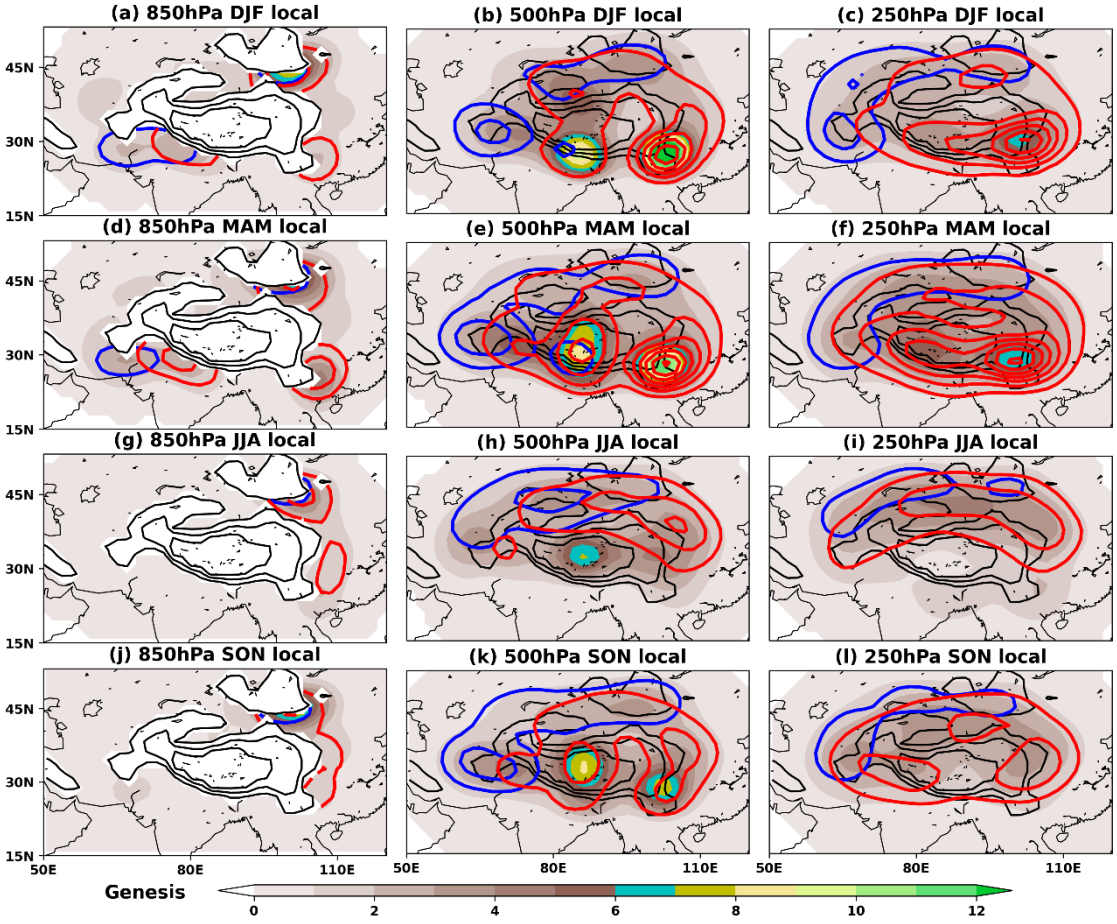

FIG. 5. Climatological (left) 850-hPa, (center) 500-hPa, and (right) 250-hPa genesis densities of locally-generated cyclones (shading) for each season: (first row) winter, (second row) spring, (third row) summer, and (fourth row) autumn. Blue (red) contours represent the genesis densities of secondary locally-generated cyclones that may be induced by the pre-existing remote (local) cyclones at the closest altitudes, which are (left) 500, (center) 250, and (right) 500 hPa. These specific vertical levels are determined from Fig. 6. Contour values are 0.5, 1, 1.5, 2, and 2.5 cyclones per month per unit area for both blue and red contours. Thick black contours indicate the elevation of 1500, 3000, and 4500 m.

In spring, as the westerly jet stream weakens, the two high genesis densities seen in DJF decrease somewhat at 500 hPa but slightly increase at 250 hPa (Figs. 5e and f). The increase in 850-hPa southeast genesis densities may be caused by the gradual increase in water vapor over this region during spring, which can supply latent heating to enhance the low-level relative vorticity (Fig. 6d). Another high genesis densities

induced by the gradually increasing TP diabatic heating appear over the central TP (Fig. 5e), but only exist at 500 hPa, signifying the high probability of these local cyclones with shallow structures, consistent with the result from other studies focusing on TP vortices (Li et al. 2014; Curio et al. 2019). All of these phenomena lead to the springtime maximized numbers of local cyclones at all three levels (Fig. 2b), indicating the strongest stimulation effect in spring. During summer, although the TP diabatic heating is maximized, the high genesis densities over the central TP are weaker than those in spring, which may be related to the weaker and more northly located westerly jet stream (Fig. 5h) (Curio et al. 2019). The preferred genesis regions at 250 hPa move with the westerly jet stream to the north of the TP (Fig. 5i). High genesis densities at all three levels disappear over the southeastern TP (third row in Fig. 5), further suggesting that their appearance is associated with the interaction between the westerly jet stream and the southeastern TP. The cyclone formation in autumn is similar to that in spring but with a weaker magnitude (fourth row in Fig. 5), consistent with the seasonal variations of the westerly jet stream.

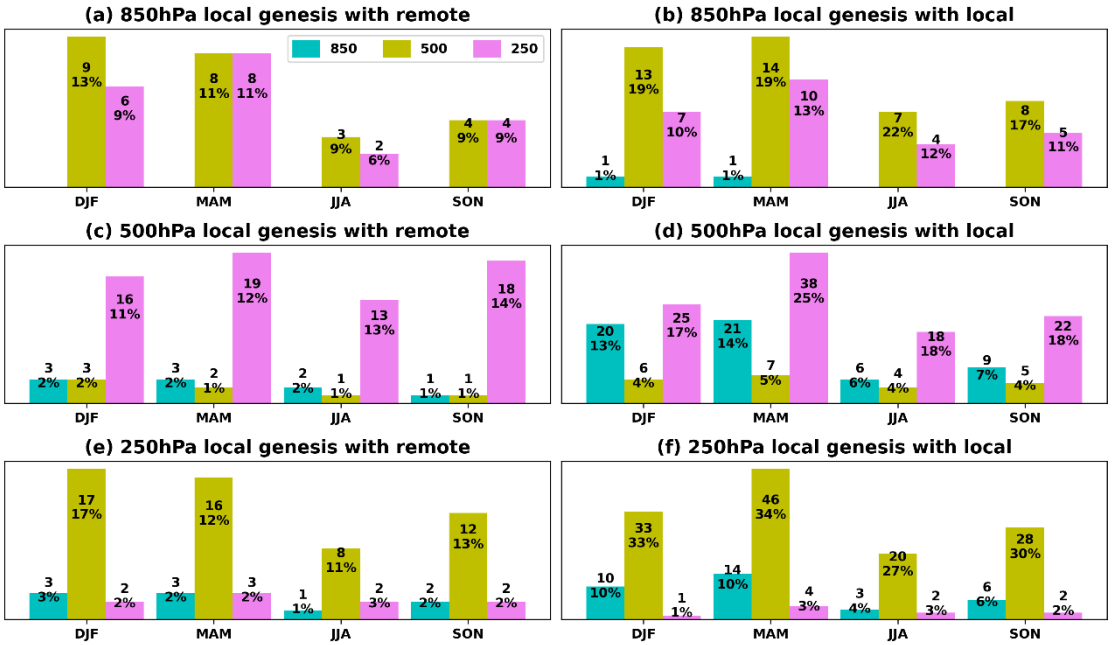

FIG. 6. Seasonal numbers of (upper) 850-hPa, (middle) 500-hPa, and (bottom) 250-hPa local cyclogenesis accompanied with the pre-existing (left) remote and (right) local cyclones at 850 hPa (cyan bars), 500 hPa (yellow bars), and 250 hPa (purple

bars). The numbers and their percentages relative to the total locally-generated cyclones at each level for each season are marked on each bar.

As is well-known, pre-existing cyclones can also trigger cyclogenesis at the same or other altitudes. For example, TP vortices are favorable for the cyclogenesis over the southwestern China through anomalous cyclonic circulations, convergence, ascending motion, and moisture transport (Li et al. 2017, 2020b). A shallow cyclone can develop into a deep cyclone under certain conditions and thus induce cyclogenesis at other altitudes. Westerly trough moving from the upstream can split into small-scale westerly troughs to the north and south of TP (Qian and Jiao 1995). To estimate the contributions of pre-existing remote and local cyclones to the cyclogenesis over the TP, an accompanied local cyclone is defined if other cyclones pass within 6 degrees of its starting point at the moment of its formation. Contours shown in Fig. 5 refer to the 850, 500, and 250-hPa genesis densities of these cyclones that may be induced by the pre-existing cyclones at 500, 250, and 500 hPa, respectively. For example, blue contours in Fig. 5a suggest that some 850-hPa local cyclogenesis to the southwestern TP may be induced by 500-hPa remote cyclones. Contributions of the pre-existing cyclones at other levels are estimated in Fig. 6, which are lower than those shown in Fig. 5, suggesting that local cyclogenesis is more likely to be induced by the pre-existing cyclones at the closest altitudes.

Left column in Fig. 6 shows that no matter at which levels and which seasons, only around 10% of local cyclogenesis may be contributed by remote cyclones, which are located over the western and northern parts of the TP (blue contours in Fig. 5). The contributions of pre-existing local cyclones to local cyclogenesis are around 20%, even up to 30% at 250 hPa (right column in Fig. 6), higher than those of remote cyclones, implying that some local cyclones may be indirectly caused by the TP. The preferred regions of these secondary local cyclogenesis are over the southeastern and central TP during all seasons except summer (red contours in Fig. 5). Local cyclogenesis accompanied by pre-existing local cyclones occurs more frequently in spring than in winter, which may be related to the slightly weaker westerly jet stream allowing

cyclones more time to develop into other altitudes. This may be used to justify the slight increase in the 250-hPa genesis densities over the southeastern TP in spring (Fig. 5f). If the accompanied local cyclone is defined by the distance of 3 degrees between the pre-existing cyclones and the cyclogenesis over the TP, the contributions of pre-existing cyclones to local cyclogenesis decrease, but their relative magnitude distribution and seasonal variations (not shown) are similar to those shown in Figs. 5 and 6.

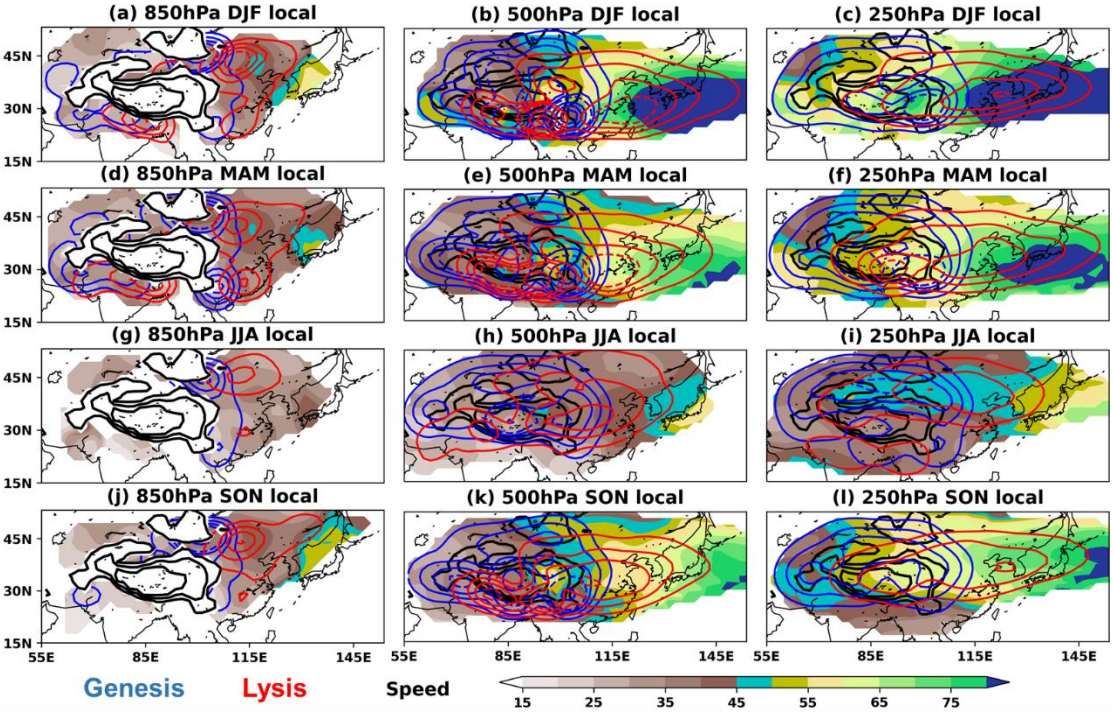

FIG. 7. As in Fig. 3, but for locally-generated cyclones around the TP.

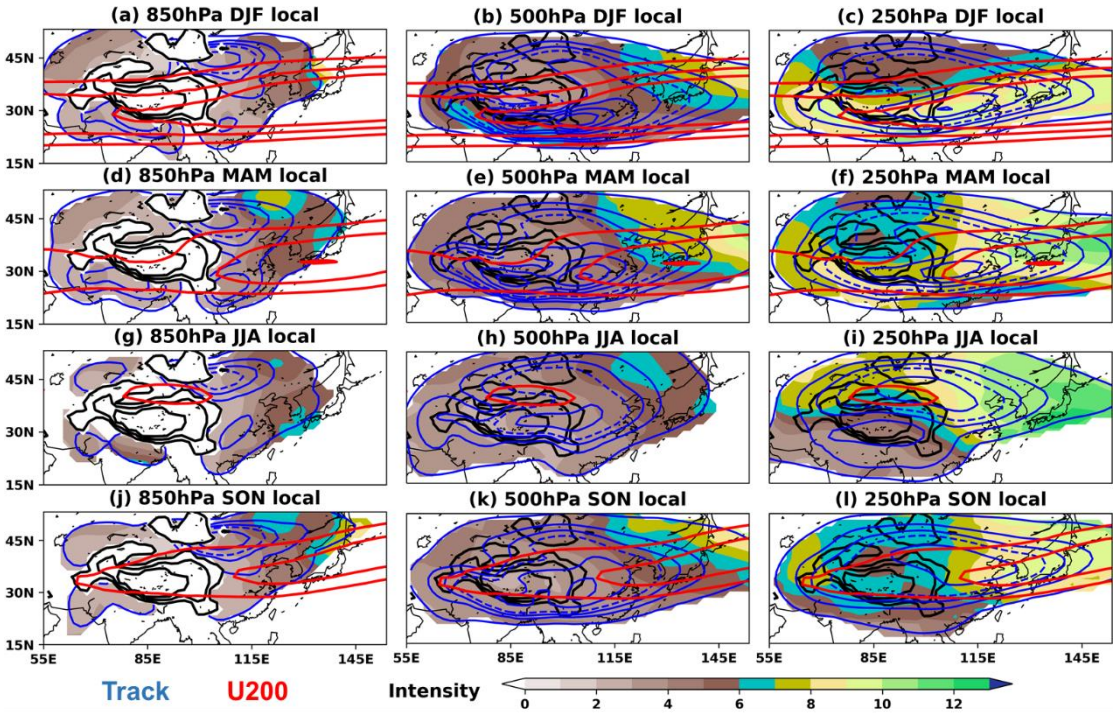

FIG. 8. As in Fig. 4, but for locally-generated cyclones.

The basic characteristics of local cyclones have also been examined in Figs. 7 and 8. High lysis densities to the south of the TP nearly overlap with the high genesis densities, showing the short lifetime and short moving distance of these cyclones generated by the frictional cyclonic shear (Figs. 7a-f). These cyclones can still contribute a large part to the 500-hPa high track densities to the south of the TP (Figs. 8b and e). Cyclones forming over the leeside of the TP and the Mongolian plateau are more likely to move northeastward and southeastward, forming two bands of high track density to the north and south of East Asia. These two bands converge near the Yellow Sea at the middle and high levels during winter and spring, implying the long traveling distances of these cyclones (Figs. 8b, c, e, and f). Consistent with the seasonal variations of the genesis densities, the 500-hPa southern band of high track density moves to the central TP during summer, different from that at other levels, again signifying that these local cyclones possess predominantly shallow vertical structures, as is known for TP vortices. Due to the slow background flow in summer, the distances traveled by the local cyclones are significantly shorter than those in other seasons (third rows in Figs. 7 and 8).

Similar to the behaviors of remote cyclones, the mean moving speeds of local cyclones are also influenced by the background flow, which increase with altitude and maximize in winter (shading in Fig. 7). The mean intensities of the southern branch, co-located with the westerly jet stream, are stronger than those of the northern branch at the middle and high levels during winter and spring. However, the northern branch at all levels can undergo a significant intensification downstream during all seasons, similar to the northern remote cyclones. During summer and autumn, the northern branch is stronger than the southern branch due to the poleward shift of atmospheric baroclinicity (shading in Fig. 8). Clearly, the intensities of the local cyclones over the TP are weaker than those of the remote cyclones over the TP or upstream (Figs. 4 and 8).

4. Summary and discussion

While previous studies were mainly focused on the effects of the TP on the westerly trough or TP vortices, in this study the effects of the plateau on all kinds of remote and local cyclones during all four seasons are comprehensively presented and compared using an objective feature tracking algorithm. Similar to the diversion effect of the TP on the wintertime circulation (Wu et al. 2007), the TP also tends to change the moving directions of remote cyclones when they approach the TP, leading to the northern and southern bands of high track densities. Only some northern cyclones move into East Asia. This diversion effect decreases with altitude, and thus some 250-hPa cyclones can directly pass over the TP from the west to the east. The TP also exhibits a suppression effect on remote cyclones, reflected in the decrease in track densities over the plateau and the suddenly-weakened moving speeds and intensities of remote cyclones upstream of the TP. Over 70% of these remote cyclones dissipate over the TP regardless of the altitude, which slightly decreases to around 65% during summer, implying a weak summertime suppression effect. This weak suppression effect is also manifested by the small decreases in the moving speeds and intensities of summertime remote cyclones when they encounter the TP. The diversion effect also becomes weakened in summer

since the main trajectories of remote cyclones move with the westerly jet stream to the north of the TP.

On the other hand, the TP also plays a strong stimulation effect on local cyclogenesis mainly through its dynamic forcing in winter, thermodynamic forcing in summer, and both forcings in the transitional seasons. Dynamic forcing, associated with the westerly jet stream, tends to induce cyclones over the southeastern corner and the southernmost border of the TP, while thermodynamic forcing favors the formation of cyclones over the central TP. Due to the relatively strong westerly jet stream and the gradually-enhanced TP thermodynamic forcing in spring, the stimulation effect of the TP in spring is stronger than that in winter. This effect is minimized in summer when the dynamic forcing of the TP weakens. The genesis densities of local cyclones are maximized just above the TP during all seasons. Their track densities also vary with altitude, reflecting the fact that most of these local cyclones are shallow, consistent with the vertical configuration of TP vortices. Moreover, around 10% of local cyclogenesis may be induced by the remote cyclones at the closest altitudes, and about 20% by the vertically closest pre-existing local cyclones, both of which may not be directly induced by the TP.

There are many more local cyclones than remote cyclones during all seasons (Fig. 2). Although about half of these local cyclones dissipate over the TP, the total number of cyclones that move off the TP, including both remote and local cyclones, are significantly more than the cyclones that enter the plateau, especially at the low and middle levels (Fig. 9). The differences range from 0 to 6 cyclones per month. According to the downstream development theory (Zurita-Gotor and Chang 2005), these moving-off cyclones can develop into strong cyclones that play an important role in the downstream weather and climate. This situation is reversed only at upper level in winter, with the differences of about 7 cyclones per month (Fig. 9c), which may be caused by the slightly weaker stimulation effect on the 250-hPa local cyclogenesis and the stronger suppression effect on the remote cyclones in winter. This phenomenon is similar to the result shown in the Fig. 6 of Penny et al. (2010), hinting a possible role of the TP in the midwinter suppression of the North Pacific storm track that mainly

occurs at the upper level (Hoskins and Hodges 2019). In a word, the TP does not significantly decrease the total cyclone numbers in most cases. However, since local cyclones are weaker than remote cyclones, the TP still exerts a suppression effect on the intensities of total cyclones around the plateau, which becomes weaker in summer (Fig. 10).

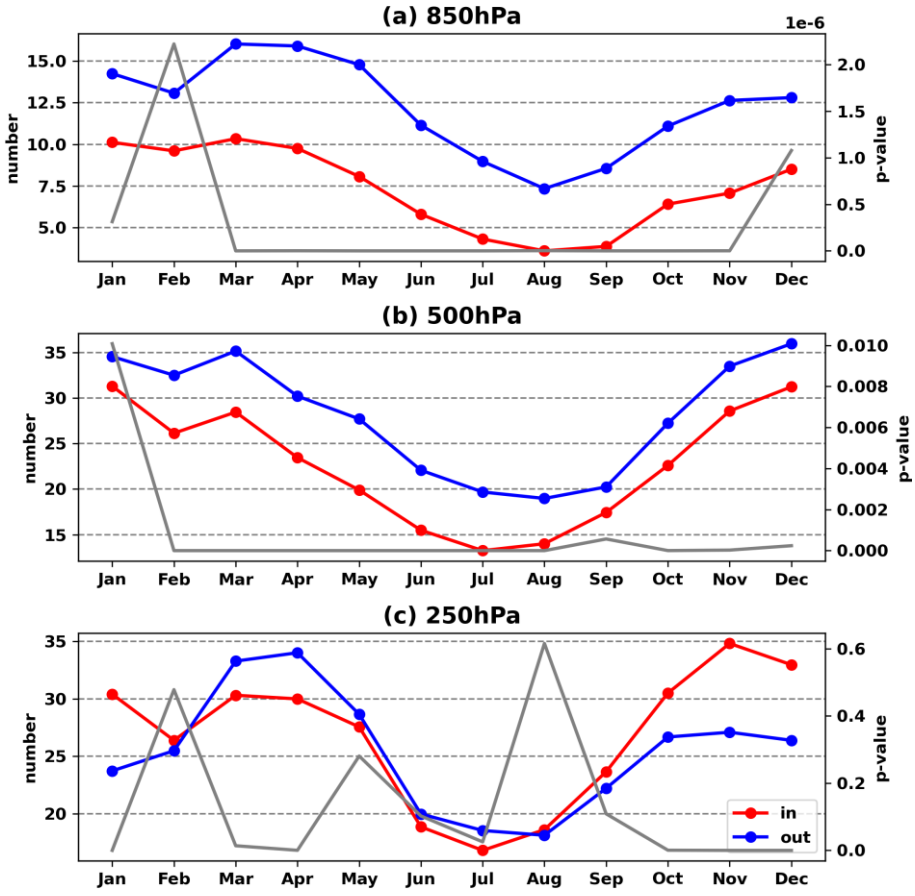

FIG. 9. Averaged monthly numbers (left y-axis) of (a) 850-hPa, (b) 500-hPa, and (c) 250-hPa cyclones moving eastward into (red) and out of (blue) the TP region. Gray lines show the probability values (right y-axis). When the probability is less than 0.01, number difference between moving-in and -off cyclones significantly exceeds the 99% confidence level of Student's two-sided *t* test.

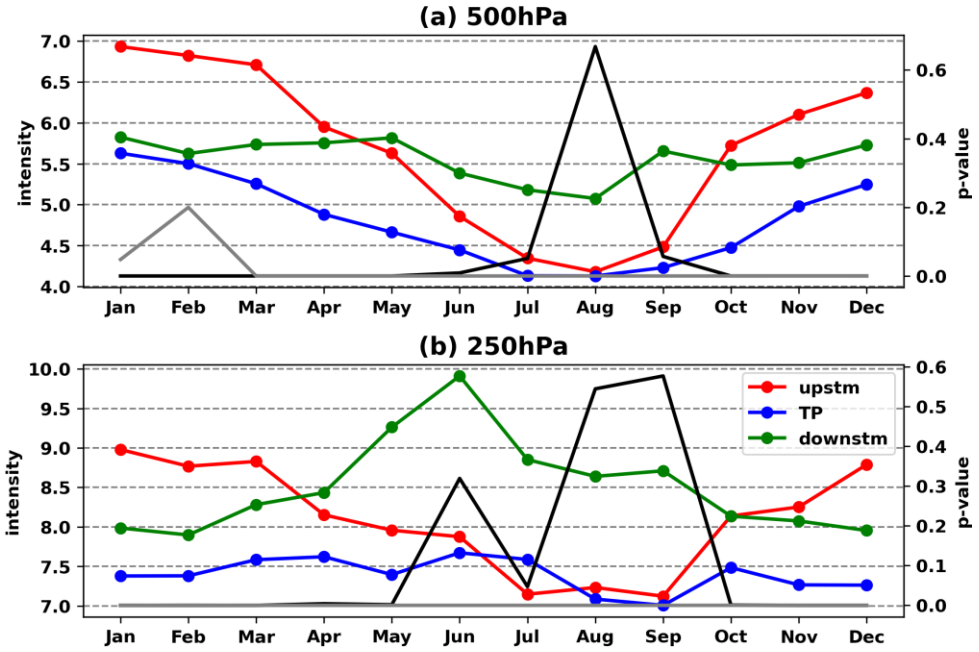

590

591 **FIG. 10.** Mean intensity (left y-axis, unit: $10^{-5}\ s^{-1}$) of (a) 500-hPa, and (c) 250-hPa
592 cyclones appearing over the TP (20~55°N/65~105°E, blue line), upstream of the TP
593 (20~55°N/40~65°E, red line), and downstream of the TP (20~55°N/105~130°E, green
594 line). Gray (black) lines show the probability values (right y-axis) of getting a result
595 that the mean intensity of cyclones over the TP is similar to that over the downstream
596 (upstream).

597

598 Considering that cyclones are the main systems that induce extreme weather
599 processes such as rainstorms, windstorms, and cold-air outbreak, this study can provide
600 a coherent reference for studying the roles played by the TP in the surrounding extreme
601 weather processes and is conducive to the predictability of extreme weather around the
602 plateau. It is well-known that cyclones are three-dimensional systems, whose vertical
603 structure may display multiple configurations during their lifetimes. They may
604 vertically extend from 850 hPa to 500 hPa at the initial stage, from 850 hPa to 200 hPa
605 at the mature stage, and finally only exist at 200 hPa, or reversed (Schwierz and Davies
606 2003; Li et al. 2020a). Nevertheless, the above analysis is a simple study of the
607 behaviors of cyclones at different pressure levels, neglecting the variations of vertical
608 structure when these cyclones move into or off the TP, which needs more investigations
609 in the future.

Acknowledgments. The authors thank Editor Dr. Yi Deng and the two anonymous reviewers for providing thorough and insightful reviews of the early versions of the manuscript. They also thank Prof. Jianhua Lu of the Sun Yat-sen University for helpful discussions. This research was supported by the Guangdong Major Project of Basic and Applied Basic Research (Grant 2020B0301030004), the National Natural Science Foundation of China (Grants 42088101, 42175023, and 41975074), the Innovation Group Project of Southern Marine Science and Engineering Guangdong Laboratory (Zhuhai) (Grant 311021001), the Guangdong Province Key Laboratory for Climate Change and Natural Disaster Studies (2020B1212060025), and the China Scholarship Council Joint Ph.D. Training Program.

Data Availability Statement. The ERA5 data was retrieved from https://cds.climate.copernicus.eu/cdsapp#!/dataset/reanalysis-era5-pressure-levels?tab=overview.

627 REFERENCES

628 Cannon, F., L. M. V. Carvalho, C. Jones, and J. Norris, 2016: Winter westerly
629 disturbance dynamics and precipitation in the western Himalaya and Karakoram:
630 a wave-tracking approach. *Theor. Appl. Climatol.*, **125**,
631 https://doi.org/10.1007/s00704-015-1489-8.
632 Chang, E. K. M., 2009: Diabetic and orographic forcing of northern winter stationary
633 waves and storm tracks. *J. Clim.*, **22**, 670–688,
634 https://doi.org/10.1175/2008JCLI2403.1.
635 ——, and W. Lin, 2011: Comments on "the role of the central Asian mountains on the
636 midwinter suppression of North Pacific storminess." *J. Atmos. Sci.*, **68**, 2800–
637 2803, https://doi.org/10.1175/JAS-D-11-021.1.
638 ——, S. Lee, and K. L. Swanson, 2002: Storm track dynamics. *J. Clim.*,
639 https://doi.org/10.1175/1520-0442(2002)015<02163:STD>2.0.CO;2.
640 Curio, J., Y. Chen, R. Schiemann, A. G. Turner, K. C. Wong, K. Hodges, and Y. Li,
641 2018: Comparison of a Manual and an Automated Tracking Method for Tibetan
642 Plateau Vortices. *Adv. Atmos. Sci.*, **35**, 965–980, https://doi.org/10.1007/s00376-
643 018-7278-4.
644 ——, R. Schiemann, K. I. Hodges, and A. G. Turner, 2019: Climatology of Tibetan
645 Plateau vortices in reanalysis data and a high-resolution global climate model. *J.*
646 *Clim.*, **32**, 1933–1950, https://doi.org/10.1175/JCLI-D-18-0021.1.
647 Dai, P., and J. Nie, 2022: Robust Expansion of Extreme Midlatitude Storms Under
648 Global Warming. *Geophys. Res. Lett.*, https://doi.org/10.1029/2022GL099007.
649 Davis, C. A., 1997: The modification of baroclinic waves by the rocky mountains. *J.*
650 *Atmos. Sci.*, **54**, https://doi.org/10.1175/1520-
651 0469(1997)054<0848:TMOBWB>2.0.CO;2.
652 Fleming, E. L., G.-H. Lim, and J. M. Wallace, 1987: Differences between the spring
653 and autumn circulation of the Northern Hemisphere. *J. Atmos. Sci.*,
654 https://doi.org/10.1175/1520-0469(1987)044<1266:dbtsaa>2.0.co;2.
655 Guan, Q., X. Yao, Q. Li, Y. Ma, and H. Zhang, 2018: Study of a horizontal shear line
656 over the Qinghai–Tibetan Plateau and the impact of diabatic heating on its

evolution. *J. Meteorol. Res.*, https://doi.org/10.1007/s13351-018-7186-7.

Hawcroft, M. K., L. C. Shaffrey, K. I. Hodges, and H. F. Dacre, 2012: How much Northern Hemisphere precipitation is associated with extratropical cyclones? *Geophys. Res. Lett.*, **39**, https://doi.org/https://doi.org/10.1029/2012GL053866.

Hersbach, H., and Coauthors, 2020: The ERA5 global reanalysis. *Q. J. R. Meteorol. Soc.*, **146**, 1999–2049, https://doi.org/10.1002/qj.3803.

Hodges, K., A. Cobb, and P. L. Vidale, 2017: How well are tropical cyclones represented in reanalysis datasets? *J. Clim.*, **30**, https://doi.org/10.1175/JCLI-D-16-0557.1.

Hodges, K. I., 1994: A general method for tracking analysis and its application to meteorological data. *Mon. Weather Rev.*, https://doi.org/10.1175/1520-0493(1994)122<2573:AGMFTA>2.0.CO;2.

——, 1995: Feature tracking on the unit sphere. *Mon. Weather Rev.*, https://doi.org/10.1175/1520-0493(1995)123<3458:ftotus>2.0.co;2.

——, 1996: Spherical nonparametric estimators applied to the UGAMP model integration for AMIP. *Mon. Weather Rev.*, https://doi.org/10.1175/1520-0493(1996)124<2914:SNEATT>2.0.CO;2.

——, 1999: Adaptive constraints for feature tracking. *Mon. Weather Rev.*, https://doi.org/10.1175/1520-0493(1999)127<1362:acfft>2.0.co;2.

Holton, J. R., 2004: *An Introduction to Dynamic Meteorology: Fourth edition*. Academic Press, 535 pp.

Hoskins, B. J., and K. I. Hodges, 2002: New perspectives on the Northern Hemisphere winter storm tracks. *J. Atmos. Sci.*, **59**, 1041–1061, https://doi.org/10.1175/1520-0469(2002)059<1041:NPOTNH>2.0.CO;2.

Hoskins, B. J., and K. I. Hodges, 2005: A new perspective on Southern Hemisphere storm tracks. *J. Clim.*, **18**, https://doi.org/10.1175/JCLI3570.1.

——, and K. I. Hodges, 2019: The annual cycle of Northern Hemisphere storm tracks. Part I: Seasons. *J. Clim.*, **32**, 1743–1760, https://doi.org/10.1175/JCLI-D-17-0870.1.

Hunt, K. M. R., A. G. Turner, and L. C. Shaffrey, 2018: The evolution, seasonality

687 and impacts of western disturbances. *Q. J. R. Meteorol. Soc.*, **144**,
688 https://doi.org/10.1002/qj.3200.
689 Javed, A., P. Kumar, K. I. Hodges, D. V. Sein, A. K. Dubey, and G. Tiwari, 2022:
690 Does the Recent Revival of Western Disturbances Govern the Karakoram
691 Anomaly? *J. Clim.*, **35**, 4383–4402, https://doi.org/10.1175/JCLI-D-21-0129.1.
692 Jiao, Y., and Z. Qian, 1994: Studies of dynamic influence of Qinghai-Xizang Plateau
693 on the eastward moving trough in winter. Part I: Some aspects of statistical facts.
694 *Plateau Meteorol. (in Chinese)*, **13**, 153–161.
695 Kang, J. M., and S. W. Son, 2021: Development processes of the explosive cyclones
696 over the northwest pacific: Potential vorticity tendency inversion. *J. Atmos. Sci.*,
697 **76**, https://doi.org/10.1175/JAS-D-20-0151.1.
698 Lee, S. S., J. Y. Lee, K. J. Ha, B. Wang, A. Kitoh, Y. Kajikawa, and M. Abe, 2013:
699 Role of the Tibetan Plateau on the annual variation of mean atmospheric
700 circulation and storm-track activity. *J. Clim.*, https://doi.org/10.1175/JCLI-D-12-
701 00213.1.
702 Li, G., and W. Zhang, 2019: Recent advances in the research of heavy rain associated
703 with vortices and shear lines come from the Tibetan Plateau. *Torrential Rain*
704 *Disasters (in Chinese)*, **38**, 464–471, https://doi.org/10.3969/j.issn.1004-
705 9045.2019.05.008.
706 Li, L., and R. Zhang, 2023: Interdecadal Shift in Dipole Pattern Precipitation Trends
707 Over the Tibetan Plateau: Roles of Local Vortices. *Geophys. Res. Lett.*,
708 https://doi.org/10.1029/2022gl101445.
709 ——, ——, M. Wen, and L. Liu, 2014: Effect of the atmospheric heat source on the
710 development and eastward movement of the Tibetan Plateau vortices. *Tellus A*
711 *Dyn. Meteorol. Oceanogr.*, **66**, 24451, https://doi.org/10.3402/tellusa.v66.24451.
712 ——, ——, and ——, 2017: Genesis of southwest vortices and its relation to Tibetan
713 Plateau vortices. *Q. J. R. Meteorol. Soc.*, **143**, https://doi.org/10.1002/qj.3106.
714 ——, ——, and ——, 2020a: Structure characteristics of the vortices moving off the
715 Tibetan Plateau. *Meteorol. Atmos. Phys.*, https://doi.org/10.1007/s00703-019-
716 00670-z.

——, ——, P. Wu, M. Wen, and J. Duan, 2020b: Roles of Tibetan Plateau vortices in the heavy rainfall over southwestern China in early July 2018. *Atmos. Res.*, **245**, https://doi.org/10.1016/j.atmosres.2020.105059.

——, ——, M. Wen, and J. Lv, 2021: Regionally Different Precipitation Trends Over the Tibetan Plateau in the Warming Context: A Perspective of the Tibetan Plateau Vortices. *Geophys. Res. Lett.*, https://doi.org/10.1029/2020GL091680.

Liu, X., E. Ma, Z. Cao, and S. Jin, 2018: Numerical study of a southwest vortex rainstorm process influenced by the eastward movement of Tibetan Plateau vortex. *Adv. Meteorol.*, **2018**, https://doi.org/10.1155/2018/9081910.

Lorenz, D. J., and D. L. Hartmann, 2003: Eddy-zonal flow feedback in the Northern Hemisphere winter. *J. Clim.*, **16**, https://doi.org/10.1175/1520-0442(2003)16<1212:EFFITN>2.0.CO;2.

Luo, S., and L. Wei, 1985: The dynamical and synoptical analysis of the effect of the Tibetan Plateatu on a cut-off processes of the trough in May, 1979. *Plateau Meteorol. (in Chinese)*, **4**, 14–22.

Ma, T., G. Wu, Y. Liu, and J. Mao, 2022: Abnormal warm sea-surface temperature in the Indian Ocean, active potential vorticity over the Tibetan Plateau, and severe flooding along the Yangtze River in summer 2020. *Q. J. R. Meteorol. Soc.*, https://doi.org/10.1002/qj.4243.

Molnar, P., W. R. Boos, and D. S. Battisti, 2010: Orographic controls on climate and paleoclimate of Asia: Thermal and mechanical roles for the Tibetan Plateau. *Annu. Rev. Earth Planet. Sci.*, **38**, 77–102, https://doi.org/10.1146/annurev-earth-040809-152456.

Ólafsson, H., and P. Bougeault, 1997: The effect of rotation and surface friction on orographic drag. *J. Atmos. Sci.*, https://doi.org/10.1175/1520-0469(1997)054<0193:TEORAS>2.0.CO;2.

Park, H. S., J. C. H. Chiang, and S. W. Son, 2010: The role of the central Asian mountains on the midwinter suppression of North Pacific storminess. *J. Atmos. Sci.*, https://doi.org/10.1175/2010JAS3349.1.

——, S. P. Xie, and S. W. Son, 2013: Poleward stationary eddy heat transport by the

747 Tibetan Plateau and equatorward shift of westerlies during northern winter. *J.*
748 *Atmos. Sci.*, **70**, 3288–3301, https://doi.org/10.1175/JAS-D-13-039.1.
749 Peixoto, J. P., and A. H. Oort, 1992: *Physics of Climate*. American Institute of
750 Physics, 520 pp.
751 Penny, S., G. H. Roe, and D. S. Battisti, 2010: The source of the midwinter
752 suppression in storminess over the North Pacific. *J. Clim.*, **23**, 634–648,
753 https://doi.org/10.1175/2009JCLI2904.1.
754 Qian, Z., and Y. Jiao, 1995: Studies of dynamic influence of Qinghai-Xizang Plateau
755 on the eastward moving trough in winter. Part III: The analyses simulations
756 experiments results. *Plateau Meteorol. (in Chinese)*, **14**, 55–66.
757 Ren, Q., X. Jiang, Y. Zhang, Z. Li, and S. Yang, 2021: Effects of suppressed transient
758 eddies by the Tibetan Plateau on the East Asian summer monsoon. *J. Clim.*,
759 https://doi.org/10.1175/jcli-d-20-0646.1.
760 ——, W. Wei, M. Lu, and S. Yang, 2022: Dynamical analysis of the winter Middle
761 East jet stream and comparison with the East Asian and North American jet
762 streams. *J. Clim.*, **35**, 4455–4468, https://doi.org/10.1175/JCLI-D-21-0664.1.
763 Rudeva, I., and S. K. Gulev, 2007: Climatology of cyclone size characteristics and
764 their changes during the cyclone life cycle. *Mon. Weather Rev.*,
765 https://doi.org/10.1175/MWR3420.1.
766 Schiemann, R., D. Lüthi, and C. Schär, 2009: Seasonality and interannual variability
767 of the westerley jet in the Tibetan Plateau region. *J. Clim.*, **22**, 2940–2957,
768 https://doi.org/10.1175/2008JCLI2625.1.
769 Schwierz, C. B., and H. C. Davies, 2003: Evolution of a synoptic-scale vortex
770 advecting toward a high mountain. *Tellus, Ser. A Dyn. Meteorol. Oceanogr.*,
771 https://doi.org/10.1034/j.1600-0870.2003.01396.x.
772 Son, S. W., M. Ting, and L. M. Polvani, 2009: The effect of topography on storm-
773 track intensity in a relatively simple general circulation model. *J. Atmos. Sci.*, **66**,
774 393–411, https://doi.org/10.1175/2008JAS2742.1.
775 Studholme, J., A. V. Fedorov, S. K. Gulev, K. Emanuel, and K. Hodges, 2022:
776 Poleward expansion of tropical cyclone latitudes in warming climates. *Nat.*

Geosci., https://doi.org/10.1038/s41561-021-00859-1.

Wang, B., 1954: The formation and development of dynamic cyclones in China under the influence of the Tibetan Plateau. *J. Shandong Univ. (in Chinese)*, **4**, 94–110.

Wang, B., 1987: The development mechanism for Tibetan Plateau warm vortices. *J. Atmos. Sci.*, **44**, 2978–2994, https://doi.org/10.1175/1520-0469(1987)044<2978:tdmftp>2.0.co;2.

Wang, Q. W., and Z. M. Tan, 2014: Multi-scale topographic control of southwest vortex formation in Tibetan plateau region in an idealized simulation. *J. Geophys. Res.*, https://doi.org/10.1002/2014JD021898.

Wu, G., and Coauthors, 2007: The influence of mechanical and thermal forcing by the Tibetan Plateau on Asian climate. *J. Hydrometeorol.*, **8**, 770–789, https://doi.org/10.1175/JHM609.1.

——, Y. Liu, B. He, Q. Bao, A. Duan, and F.-F. Jin, 2012: Thermal controls on the Asian summer monsoon. *Sci. Rep.*, **2**, https://doi.org/10.1038/srep00404.

——, and Coauthors, 2015: Tibetan Plateau climate dynamics: Recent research progress and outlook. *Natl. Sci. Rev.*, **2**, 100–116, https://doi.org/10.1093/nsr/nwu045.

Yeh, T., 1952: The seasonal variation of the influence of Tibetan Plateau on the general circulation. *Acta Meteorol. Sin. (in Chinese)*, **23**, 33–47.

Yu, J. Y., and D. L. Hartmann, 1995: Orographic influences on the distribution and generation of atmospheric variability in a GCM. *J. Atmos. Sci.*, https://doi.org/10.1175/1520-0469(1995)052<2428:oiotda>2.0.co;2.

Zappa, G., M. K. Hawcroft, L. Shaffrey, E. Black, and D. J. Brayshaw, 2015: Extratropical cyclones and the projected decline of winter Mediterranean precipitation in the CMIP5 models. *Clim. Dyn.*, https://doi.org/10.1007/s00382-014-2426-8.

Zhang, G., J. Mao, Y. Liu, and G. Wu, 2021: PV Perspective of Impacts on Downstream Extreme Rainfall Event of a Tibetan Plateau Vortex Collaborating with a Southwest China Vortex. *Adv. Atmos. Sci.*, https://doi.org/10.1007/s00376-021-1027-9.

807 Zhang, Y., L. Yang, D. Xiaokaiti, H. Qin, Y. Li, and X. Yang, 2012: The central
808 Asian vortexes activity during 1971—2010. *J. Appl. Meteorol. Sci. (in Chinese)*,
809 **23**, 312–321, https://doi.org/10.3969/j.issn.1001-7313.2012.03.007.
810 Zhao, Y., L. Fu, C. F. Yang, and X. F. Chen, 2020: Case study of a heavy snowstorm
811 associated with an extratropical cyclone featuring a back-bent warm front
812 structure. *Atmosphere (Basel).*, **11**, https://doi.org/10.3390/atmos11121272.
813 Zhuang, X., R. Li, B. Li, J. Li, and Z. Sun, 2017: Analysis on rainstorm caused by
814 central Asian vortex in northern Xinjiang. *Meteorol. Mon. (in Chinese)*, **43**, 924–
815 935, https://doi.org/10.7519/j.issn.1000-0526.2017.08.003.
816 Zurita-Gotor, P., and E. K. M. Chang, 2005: The impact of zonal propagation and
817 seeding on the eddy-mean flow equilibrium of a zonally varying two-layer
818 model. *J. Atmos. Sci.*, **62**, https://doi.org/10.1175/JAS3473.1.
819